


# Preoperative and postoperative high angular resolution diffusion imaging tractography of cerebellar pathways in posterior fossa tumors

Alpen Ortug<sup>1,2</sup>  | Neslihan Yuzbasioglu<sup>1</sup> | Nejat Akalan<sup>3</sup> | Jacob Levman<sup>4</sup> | Emi Takahashi<sup>2</sup>

<sup>1</sup>Department of Anatomy, School of Medicine, Istanbul Medipol University, Istanbul, Turkey

<sup>2</sup>Division of Newborn Medicine, Boston Children's Hospital, Harvard Medical School, Boston, Massachusetts, USA

<sup>3</sup>Department of Neurosurgery, School of Medicine, Istanbul Medipol University, Istanbul, Turkey

<sup>4</sup>Department of Computer Science, St. Francis Xavier University, Antigonish, Nova Scotia, Canada

## Correspondence

Alpen Ortug, Athinoula A. Martinos Center for Biomedical Imaging, Massachusetts General Hospital, Charlestown, Massachusetts, USA.  
Email: [aortug@mgh.harvard.edu](mailto:aortug@mgh.harvard.edu)

## Present address:

Alpen Ortug and Emi Takahashi, Athinoula A. Martinos Center for Biomedical Imaging, Massachusetts General Hospital, Charlestown, Massachusetts, USA.  
Alpen Ortug and Emi Takahashi, Department of Radiology, Harvard Medical School, Boston, Massachusetts, USA.

## Funding information

National Institutes of Health, Grant/Award Numbers: R01HD078561, R01NS109475; Research Fund of Istanbul Medipol University, Grant/Award Number: 2018/14

## Abstract

This study aimed to utilize high angular resolution diffusion magnetic resonance imaging (HARDI) tractography in the mapping of the pathways of the cerebellum associated with posterior fossa tumors (infratentorial neoplasms) and to determine whether it is useful for preoperative and postoperative evaluation. Retrospective data from 30 patients (age 2–16 yr) with posterior fossa tumor (17 low grade, 13 high grade) and 30 age-sex-matched healthy controls were used. Structural and diffusion-weighted images were collected at a 3-tesla scanner. Tractography was performed using Diffusion Toolkit software, Q-ball model, FACT algorithm, and angle threshold of 45 degrees. Manually assessed regions of interest were placed to identify reconstructed fiber pathways passing through the superior, medial, and inferior cerebellar peduncles for the preoperative, postoperative, and healthy control groups. Fractional anisotropy (FA), apparent diffusion coefficient (ADC), and track volume measures were obtained and analyzed. Statistically significant differences were found between the preop/postop, preop/control, and postop/control comparisons for the volume of the tracts in both groups. Displacement and disruption of the pathways seemed to differ in relation to the severity of the tumor. The loss of pathways after the operation was associated with selective resection during surgery due to tumor infiltration. There were no FA differences but significantly higher ADC in low-grade tumors, and no difference in both FA and ADC in high-grade tumors. The effects of posterior fossa tumors on cerebellar peduncles and reconstructed pathways were successfully evaluated by HARDI tractography. The technique appears to be useful not only for preoperative but also for postoperative evaluation.

## KEYWORDS

cerebellum, diffusion magnetic resonance imaging, infratentorial neoplasms

## 1 | INTRODUCTION

The formation and growth of a tumor in the infratentorial region may result in damage to the structures in this region and are often

associated with hydrocephalus (Packer et al., 2002). The tumors located in the infratentorial region are called posterior fossa tumors, which are more common in children compared to adults (Prasad et al., 2017). Approximately 44%–70% of childhood brain tumors are

supratentorial, and 30%–56% are infratentorial (Albright, 1992; Black, 2000). Astrocytomas, medulloblastomas, and ependymomas are the most common among posterior fossa tumors. However, dermoid tumors, rhabdoid tumors, teratomas, and rarely high-grade glial tumors, meningiomas, and metastasis can also be encountered (Packer et al., 2002). The presence of the tumor may lead to edema, infiltration, displacement, or disruption in the white matter tracts (Witwer et al., 2002; Yen et al., 2009).

Diffusion-weighted imaging (DWI) is a magnetic resonance technique sensitive to the movement of water molecules that allows the detection of white matter pathways with three-dimensional spatial localization in normal and/or pathologically interrupted situations (Lope-Piedrafita, 2018), and can be used in vivo. Conventional structural MRI (e.g., T2-weighted MRI) can accurately identify the size and the mass of the tumor, but appear normal in areas with tumor invasion without detailed information about the integrity of the white matter and the tumor, while diffusion MRI can provide information about abnormalities in the white matter and tumor in patients with malignant tumors (Bulakbasi, 2009). Diffusion tensor imaging (DTI) analyzes the three-dimensional shape of diffusion (Huisman, 2010). DTI is used to differentiate high- from low-grade brain tumors, help to plan radiotherapy target volume, and determine the tumor margins for surgery (Yen et al., 2009). It has become an important component of a multifaceted approach to preoperative intraoperative planning and decision making (Essayed et al., 2017). DTI is important to preoperatively identify the location and the integrity of the tumor, as well as the condition of neighboring white matter pathways, in order to accurately plan a surgical operation (Karimi et al., 2006). Using diffusion MRI tractography, it has been possible to provide a safer and patient-specific procedure by imaging important fiber tracts in the brain such as the corticospinal tract and arcuate fasciculus, around which the neurosurgeon could not access tumors without direct electrical stimulation previously (Potgieser et al., 2014; Salama et al., 2017). Diffusion MRI also allows visualization of changes after the operation that are caused by the tumor on the tracts during a recovery phase (Dubey et al., 2018).

Many researchers no longer consider DTI as the golden standard for tractography obtained via DWI (Farquharson et al., 2013; Salama et al., 2017). A limitation of DTI is that the diffusion tensor model cannot accurately reveal the complex structure of crossing white matter fibers. DTI fiber tracking cannot exactly follow the white matter pathways passing through the intersections (Jin et al., 2019). For this reason, it is recommended to use the high angular resolution diffusion imaging (HARDI) / Q-ball method, which is another method for fiber tracking from diffusion imaging, which provides more accurate results, especially in regions with crossing fibers (Berman et al., 2013; Jin et al., 2019; Re et al., 2017; Tuch, 2004). HARDI has the feature of distinguishing multiple fiber assemblages crossing the same voxel (Tuch, 2004). While the fiber tracking HARDI method can follow the white matter pathways through the regions crossing the fibers, the classical DTI fiber tracking process stops in the same regions or gives erroneous results (Berman et al., 2013). However, the use of HARDI in clinical sciences is still less frequently used than that of DTI due to the relatively new nature of the method (Salama et al., 2017).

DTI has been used to investigate cerebral and/or cerebellar tracts in healthy individuals (Kamali et al., 2010; Keser et al., 2015) and those with various neurological diseases (Akhlaghi et al., 2014; Tae et al., 2018). Additionally, there are a few studies with types of brain neoplasms (Celtikci et al., 2018; Ibrahim et al., 2013; Ma et al., 2016; Price et al., 2003; Yen et al., 2009), focusing on the long-term effects of childhood posterior fossa tumors on survivors (McEvoy et al., 2016; Oh et al., 2017; Vedantam et al., 2019) or only before the treatment of posterior fossa tumors (Assis et al., 2015). However, no study has been reported to examine posterior fossa tumors with their subtypes, preoperative features, and cortical extensions, and evaluate tractography preoperatively and postoperatively comparing with matching healthy controls. Also, no other study was found to determine any positive or negative change postoperatively. This study aims to demonstrate the role of HARDI tractography in the mapping of the cerebellar pathways associated with posterior fossa tumors and determine whether HARDI is useful for brain surgery planning and postoperative evaluation.

## 2 | PATIENTS AND METHODS

Following approval by Boston Children Hospital's (BCH) Institutional Review Board (informed consent was waived due to the lack of risk to participants included in this retrospective analysis), the clinical imaging electronic database at BCH was reviewed for the present analysis from January 01, 2008 to February 24, 2016 and collected MRI data of patients and controls. An analysis was conducted on those patients who, according to the records, had posterior fossa tumor, underwent surgery in this hospital and were followed up in this hospital after surgery. All types of infratentorial tumors were included in the study list regardless of the pathology. A total of 296 patients' medical reports were examined. According to the available data, a chart was prepared regarding the patients' age, sex, preoperative diagnosis, postoperative clinical evaluations, tumor localization, and pathology results. Accordingly, a total of 40 patients were eligible for inclusion in the study. It was not possible to use all images because of technical reasons such as extreme movement, low quality, lack of diffusion MRI or postoperative scanning. Up to 3 months post-surgery was used for postoperative control scanning, while any scanning later than that was excluded.

As a result, 30 patients (18 males and 12 females) with T1w, T2w, FLAIR scans and a DWI sequence with either 30 or 35 directions (described below) were included for the study. Also, to increase the reliability of the study, a healthy age-sex matched control group was included (30 healthy controls, 18 males, and 12 females). Among the control subjects, the leading reasons for the MRI examinations were headaches, to rule out intracranial pathologies, vomiting, and night awakenings. The table showing the grades and pathology of the included subjects are given in Table 1. Tumor grade I-II grouped as 'low-grade' (n:17) and grade III-IV grouped as 'high-grade' (n: 13). A list of the subjects' age-sex, pathology, and site of tumor information is given in Table 2.

**TABLE 1** Included subjects with different grades and pathology.

Grade	Glioma's				Other		
	Ependymoma	Astrocytoma	Medulloblastoma	Undefined	Ewing sarcoma	Ganglioglioma	Choroid plexus papilloma
(Grade I-II)	1	14	–	–	–	1	1
(Grade III)	2	1	–	–	–	–	–
(Grade IV)	–	–	8	1	1	–	–

## 2.1 | Acquisition parameters of diffusion weighted images

For dMRI and tractography, sequences were obtained with four clinical 3 T MRI scanners of the same manufacturer, 30 or 35 different diffusion directions ( $b = 1000\text{--}1050\text{ s/mm}^2$ ), 1 to 10 non-directional diffusion-weighted volumes ( $b = 0\text{ s/mm}^2$ ) (Siemens Medical Systems, Erlangen, Germany) from both posterior fossa tumor patients and controls at BCH [TR 4500–15,343 ms (mean:  $8357.76 \pm 3048.33$ ), TE 83–95 ms (mean:  $88.57 \pm 2.05$ ), FOV = 220–267 (mean:  $221.92 \pm 7.65$ ), matrix  $128 \times 128$  for most except one]. The acquisition parameters and scanners for each image are summarized in Supplementary Material S1. Spatial resolution varied in the x- and y-directions from 1.56 to 2.085 mm (mean: 1.74 mm, SD: 0.06 mm). Through-plane slice thickness varied from 2 to 4 mm (mean: 2.11 mm, SD: 0.42 mm).

## 2.2 | Tractography of the patient and healthy control groups

TrackVis (Version 0.6.1; trackvis.org) and diffusion toolkit were used to reconstruct and visualize tractography pathways. The FACT algorithm and  $45^\circ$  angle threshold were used in the HARDI (Q-ball) model to reconstruct tractography pathways. The fractional anisotropy (FA) threshold was not used for the reconstruction of fibers (Re et al., 2017). The tracts were delineated as a group with a region-of-interest (ROI) to be placed on each of the three peduncles of the cerebellum (Leitner et al., 2015; Re et al., 2017).

## 2.3 | Placement of ROIs

### 2.3.1 | Superior cerebellar peduncles (SCP) (Right–Left)

A spherical ROI was placed on the dentate nucleus at the midline of the pons on the axial FA color map. A second spherical ROI was placed on the ipsilateral superior cerebellar peduncle at the intersection of the pontomesencephalic junction with the superior cerebellar peduncle (green on the FA color map) (Figure 1A). The fibers of this pathway could not be traced towards the dorsal contralateral cortex after the transverse angle by using these tracing methods, but the fibers going to the ipsilateral cortex were traced and configured using

the method described by Mori et al. (Mori et al., 2005). These fibers revealed the nondecussating pathway of the dentato-rubro-thalamic tract passing through the superior cerebellar peduncles (Meola et al., 2016).

### 2.3.2 | Middle cerebellar peduncles (MCP)

Pontocerebellar fibers first emerge from the pontine nuclei and spreads in the anteroposterior direction (green on the FA color map) traversing the midline (red on the FA color map) before entering the cerebellum. MCP was monitored by placing two spherical ROIs in the midsections of the right and left PCM fibers in the cerebellum (Figure 1B). MCP are configured as a single pathway in healthy individuals. In the present study, however, right, and left sides were formed separately due to the presence of tumor in this region or the operation of the tumor in most of the samples. Both the individual values and the right–left averages of these data were recorded.

### 2.3.3 | Inferior cerebellar peduncles (ICP) (Right–Left)

The first ROI sphere was placed axially to the ICP at the level of the bulbous below the dentate nucleus (shown in blue on the FA color map) (Figure 1C). As described by Mori et al. (Mori et al., 2005), the second spherical ROI was placed at the pontomesencephalic junction of the ipsilateral ICP (appearing as green voxels on the FA color map). The fibers were traced from ROI1 to ROI2. The results obtained matched the data of other researchers (Leitner et al., 2015; Re et al., 2017). The reconstructed fibers revealed the dorsal spinocerebellar tract.

All three reconstructed tracts are shown in Figure 1D.

## 2.4 | Statistical analysis

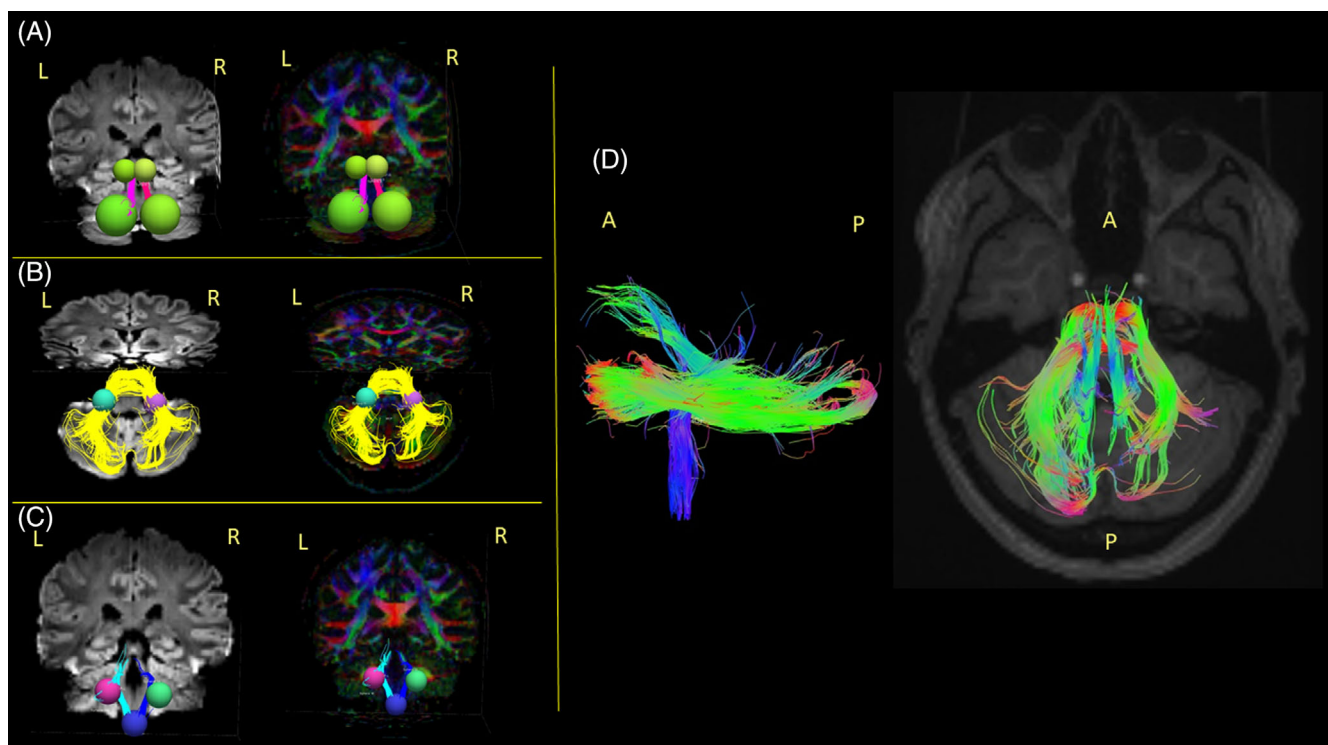
SPSS 22 (I.B.M., Chicago) software was used for statistical analysis and the bar graphs were created using the Graphpad Prism V8.0 software. The results are presented as mean values  $\pm$  SD ( $\bar{x} \pm SD$ ). The normal distribution suitability of the parameters was investigated using the Shapiro–Wilk test. The independent two-group t-test was used for intergroup evaluations of normally distributed quantitative variables, while the Paired Samples t-test was utilized for intragroup

TABLE 2 List of the patients included in the study with their corresponding preoperative symptoms and site of the lesions.

Code	Age	Sex	Pathology	Preoperative diagnosis	Site of lesion
S2	2	M	Anaplastic ependymoma	Right-sided head tilt Intermittent emesis Slightly increased fussiness Obstructive hydrocephalus	Fourth ventricular lesion arising from the roof and lateral walls with extension into the cerebellopontine angles bilaterally
S4	10	F	Medulloblastoma	Headaches Evidence of Papilledema	Fourth ventricular lesion with leptomeningeal spread
S6	8	F	Pilocytic astrocytoma	Headaches Nausea Vomiting	Fourth ventricular lesion
S7	14	M	Pilocytic astrocytoma	Right-sided hearing loss	Left cerebellar lesion
S8	8	F	Juvenile pilocytic astrocytoma	Progressive headaches Emesis	Midline cerebellar lesion
S9	15	M	Juvenile pilocytic astrocytoma	Progressive worsening headaches Nausea Vomiting	Left cerebellar lesion
S10	2	F	Juvenile pilocytic astrocytoma	Developmental delay with walking Truncal ataxia	Midline cerebellar lesion
S11	5	M	Astrocytoma	Headaches	Left cerebellar lesion
S12	2	M	Pilocytic astrocytoma	Benign macrocephaly	Right dorsolateral medulla
S13	3,5	M	Ganglioglioma	Torticollis and right head tilt Motor tics Longstanding clumsiness Truncal ataxia	Left side of the pons extending into the superior and middle cerebellar peduncles and cerebellum with irregular enhancement
S14	8	M	Medulloblastoma.	Vomiting Weight loss Headaches visual complaints Balance problem	Fourth ventricular lesion
S15	10	F	Anaplastic medulloblastoma	Intermittent headaches (primarily left-sided) Episodic Vomiting Unsteady gait Auditory hallucinations Hydrocephalus	Fourth ventricular lesion
S16	1,5	F	Anaplastic medulloblastoma	Persistent vomiting Gait ataxia Hydrocephalus	Fourth ventricular lesion
S17	13	F	Astrocytoma	Headaches Nausea Vomiting	Fourth ventricular lesion

TABLE 2 (Continued)

Code	Age	Sex	Pathology	Preoperative diagnosis	Site of lesion
S18	7	M	Ewing sarcoma	Headaches Vomiting Head tilts Hydrocephalus	Posterior fossa
S21	6	F	Pilocytic astrocytoma	Truncal ataxia Papilledema Right upper extremity dysmetria Macrocephaly Non-communicating hydrocephalus	Right cerebellar lesion
S23	16	F	Pilocytic astrocytoma	Incidentally found Mild hydrocephalus	Left cerebellar lesion
S25	15	F	High-grade glioma	Vertigo episodes Headache	Right cerebellar lesion
S26	7	M	Anaplastic medulloblastoma	Headaches Vomiting Diplopia	Posterior fossa mass with leptomeningeal spread
S28	16	F	Choroid Plexus Papilloma	Incidental finding	Fourth ventricular lesion
S29	7	F	Anaplastic astrocytoma	Vomiting Headaches Dizziness	Fourth ventricular lesion
S30	8	M	Pilocytic astrocytoma	Left spastic hemiplegia	Left cerebellar peduncles/brainstem
S33	15	M	Pilocytic astrocytoma	Regrowth of the previous resection	Right cerebellopontine angle right middle cerebral peduncle
S34	12	M	Medulloblastoma	Headaches	Fourth ventricular lesion
S35	2	M	Medulloblastoma	Incidental finding Hydrocephalus	Left cerebellar lesion
S36	2	F	Pilocytic astrocytoma	Progressive ataxia Hydrocephalus	Midline cerebellar lesion
S37	4	M	Pilocytic astrocytoma	Headaches Snoring Left facial weakness Tongue deviating to aside, some ptosis Balance issues Hypophonia	Cervicomedullary junction lesion
S38	2	M	Anaplastic ependymoma	Gait ataxia	Right cerebellar lesion
S39	1,5	M	Ependymoma	Declining motor skills Papilledema Obstructive hydrocephalus	Fourth ventricular lesion
S40	2	M	Medulloblastoma	Morning vomiting Irritability	Midline cerebellar lesion



**FIGURE 1** The reconstruction of the cerebellar fibers on a healthy control subject. (A) Right and left ROI for SCP (The nondescussating pathway of the dentato-rubro-thalamic tract). (B) Right and left ROI for MCP (Transverse pontine fibers). (C) Right and left ROI for ICP (Dorsal spinocerebellar tract). (D) Overall fibers from lateral and superior view with directional color code.

comparisons. The Mann–Whitney U test was used for intergroup comparisons of quantitative variables that did not show normal distribution, while the Wilcoxon signed-ranks test was used for intragroup comparisons. Statistical significance was considered as  $p < 0.05$ .

### 3 | RESULTS

The study was conducted with a total of 60 children, 40% ( $n = 24$ ) girls and 60% ( $n = 36$ ) boys. Thirty cases in the patient group (30 scans preoperatively and 30 scans postoperatively) and 30 cases in the control group (30 scans) were included. The groups were divided into two as low grade tumors ( $n:17$ ) and high grade tumors ( $n:13$ ).

After the three-dimensional fiber configuration reconstruction, the effects of the tumor on the cerebellar tractography pathways were determined morphologically. To evaluate the findings statistically, the FA value, apparent diffusion coefficient (ADC) value, fiber volume were recorded. Tractography examples of displacement, infiltration-selective resection, disruption with displacement and displacement of pre and post compared to healthy controls are shown in Figures 2–5.

#### 3.1 | FA evaluation

Figure 6 shows comparisons of mean FA variables between preoperative and postoperative patients and controls in both tumor groups

(Tables S1 and S2). In comparison between preoperative and postoperative in the same patient, and between patients and age- and sex-matched controls, differences in the mean FA values of MCP-R, MCP-L, MCP mean, SCP-R, SCP-L, ICP-L, ICP-R, and ALL were not statistically significant ( $p > 0.05$ ) (Figure 6).

#### 3.2 | ADC evaluation

Figure 7 shows comparisons of mean ADC variables between preoperative and postoperative patients and controls in both tumor groups (Tables S3 and S4).

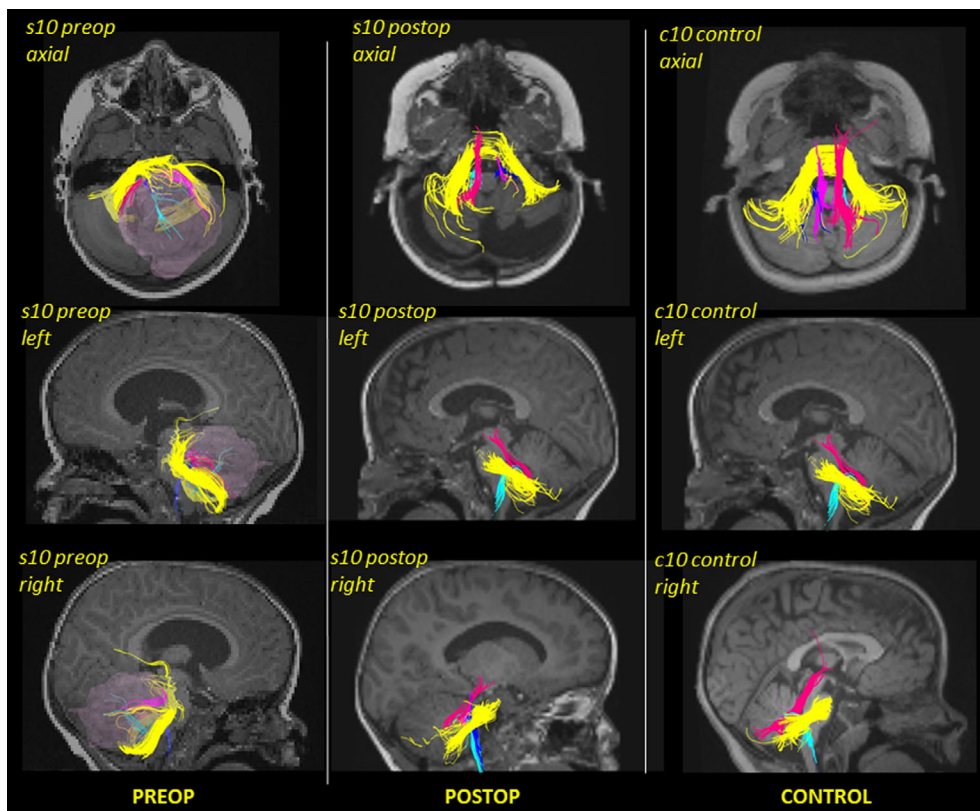
##### 3.2.1 | Evaluation of low-grade tumors

In the low-grade tumor patients' group, the Mean ADC values of MCP-R, MCP-L, MCP mean, SCP-R, SCP-L, ICP-L, ICP-R, and ALL were not statistically significantly different between the preoperative and postoperative period ( $p > 0.05$ ).

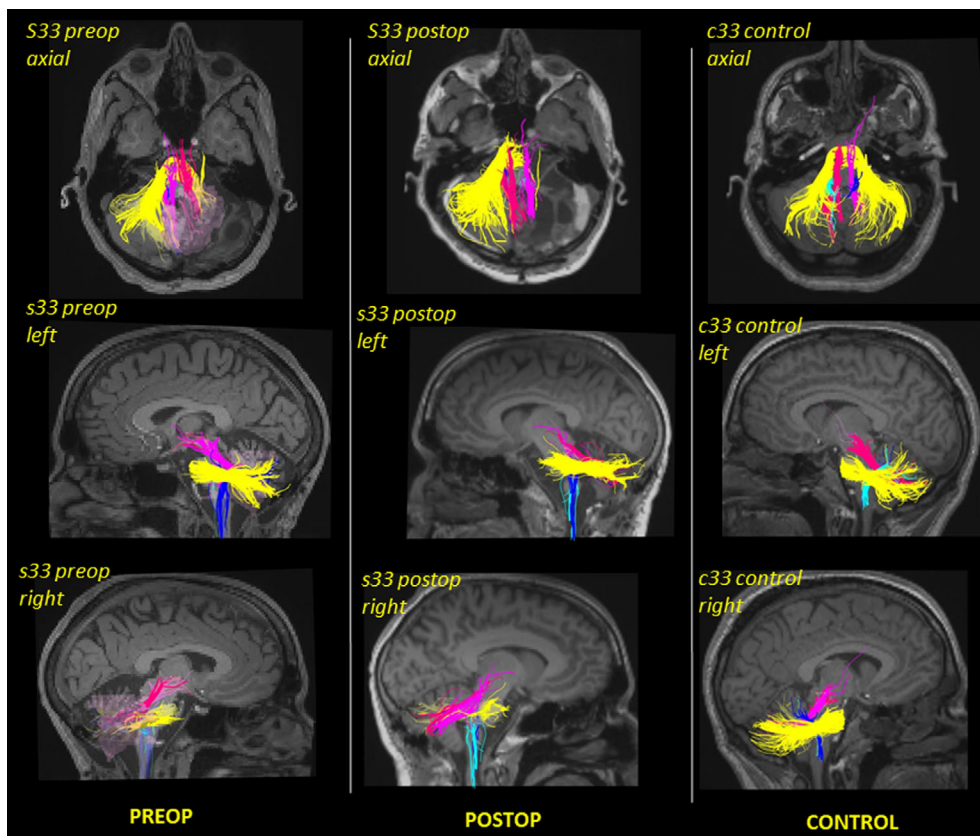
The MCP-R, MCP-L, MCP mean, SCP-R and SCP-L, and ALL values measured in the preoperative patient group were significantly higher than the control group values ( $p < 0.05$ ), while ICP-L and ICP-R measurements did not produce a statistically significant difference between the preoperative patients' values and the control group values ( $p > 0.05$ ).



**FIGURE 2** An example of displacement. The patient is a 2-years-old female, with a cerebellar tumor and the pathology was juvenile pilocytic astrocytoma. She had a presurgical developmental delay with regard to walking but also evidence of truncal ataxia.



**FIGURE 3** An example of infiltration-selective resection. The patient is a 15-years-old male, with tumor at the right cerebellopontine angle and middle cerebellar peduncle. The tumor was recurrent residual pilocytic astrocytoma. The tumor was found by follow-up MRI showing regrowth of the previously resected tumor.



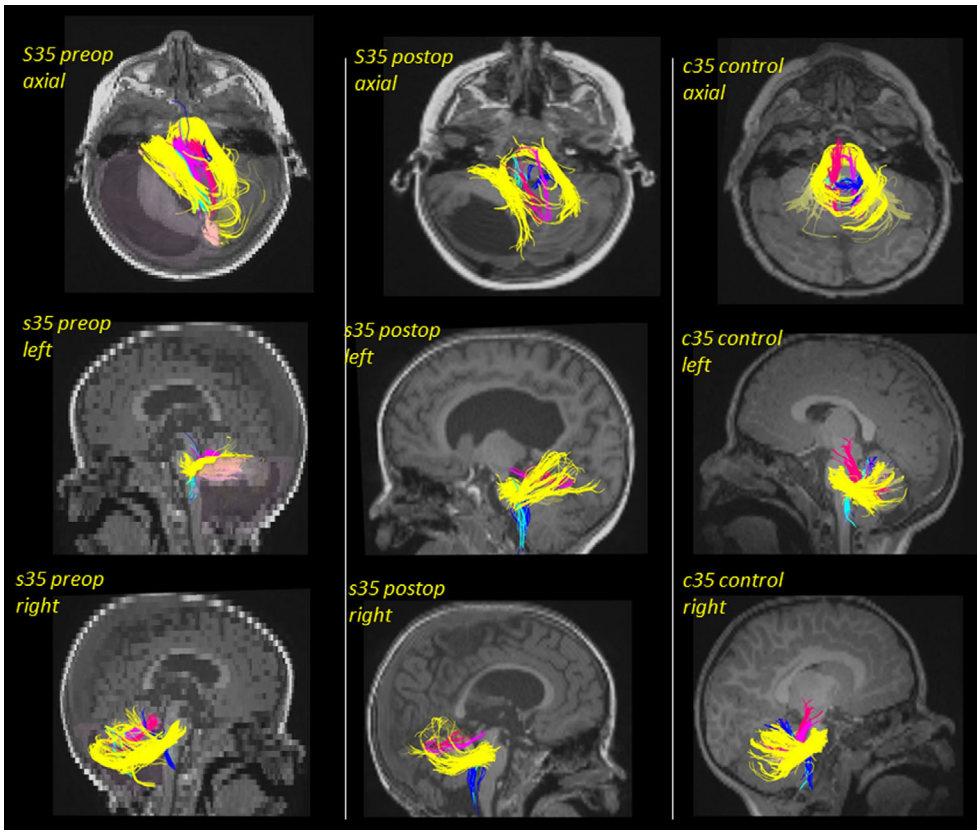


**FIGURE 4** An example of disruption with displacement. The patient is a 2-years-old, male, with a left cerebellar lesion and the pathology was medulloblastoma. This tumor was found incidentally but he suffered from persistent hydrocephalus after the surgery.

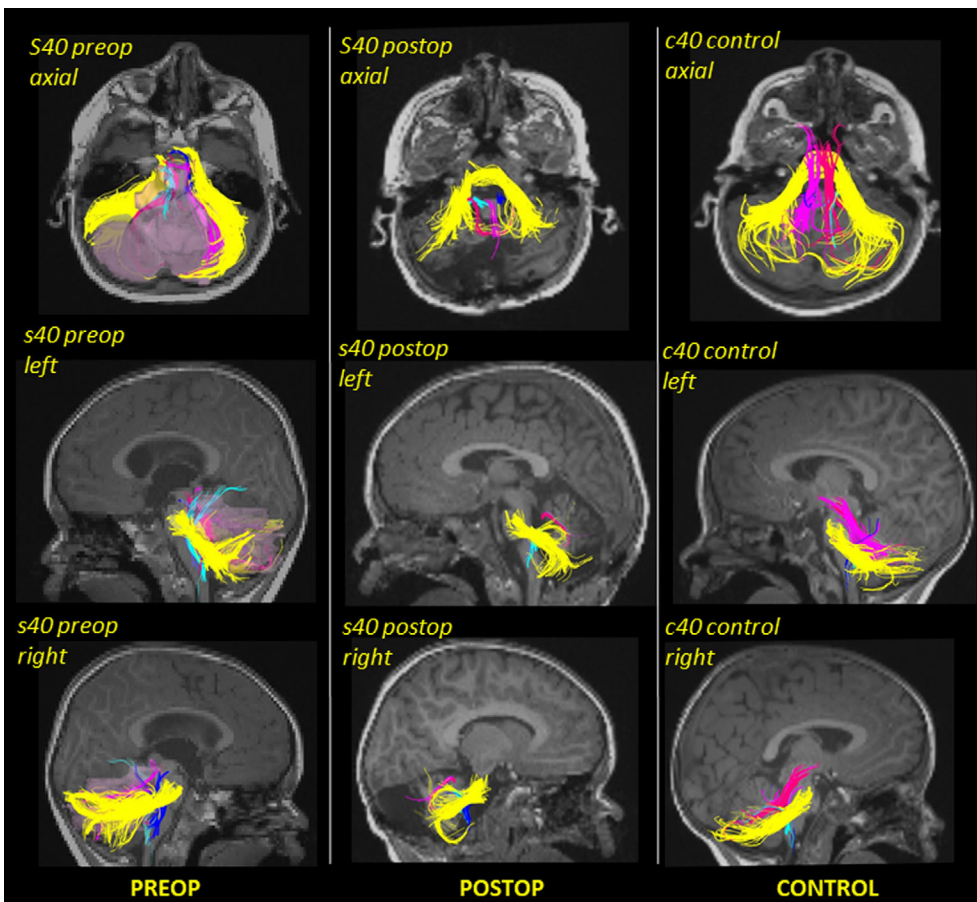
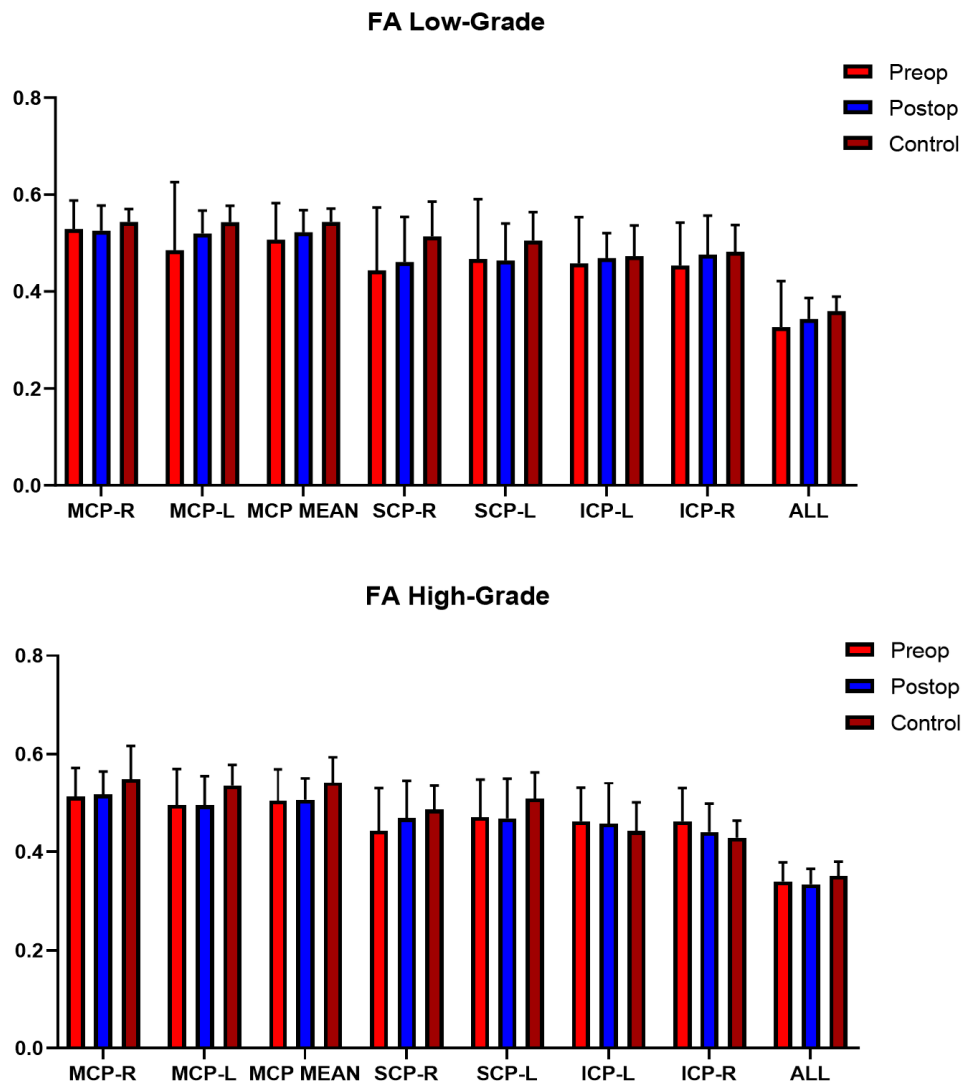


**FIGURE 5** An example of disruption with displacement. The patient is a 2-years-old, male with a midline cerebellar lesion. The pathology was medulloblastoma. He had morning vomiting and irritability before the surgery.



**FIGURE 6** The bar graph showing mean FA values of the three groups in all regions.



The MCP-L and ALL values measured in the postoperative patient group were significantly higher than control group values ( $p < 0.05$ ), while MCP-R, MCP mean, SCP-R, SCP-L, ICP-L, and ICP-R measurements did not show a statistically significant difference between the postoperative patient group values and the control group values ( $p > 0.05$ ).

### 3.2.2 | Evaluation of high-grade tumors

The mean ADC variables of MCP-R, MCP-L, MCP mean, SCP-R, SCP-L, ICP-L, ICP-R, and ALL did not produce a statistically significant difference between the preoperative patient group values and the postoperative patient group values ( $p > 0.05$ ).

## 3.3 | Fiber volume evaluation

Figure 8 shows comparisons of mean fiber volume variables between preoperative and postoperative patients and controls in both tumor groups (Tables S5 and S6).

### 3.3.1 | Evaluation of low-grade tumors

ICP-L values measured in the preoperative patient group were significantly higher than the postoperative patients, and control group values ( $p < 0.05$ ), while all other regions did not produce a statistically significant difference between the preoperative patients and the other two groups.

The MCP-L and MCP mean values measured in the control group were significantly higher than the postoperative patient group values ( $p < 0.05$ ), while all other regions did not show a statistically significant difference between the postoperative patient group values and the control group values ( $p > 0.05$ ).

### 3.3.2 | Evaluation of high-grade tumors

The MCP-R, MCP-L, MCP mean, and ICP-L values measured in the preoperative patient group were significantly higher than the preoperative patient group values ( $p < 0.05$ ). However, SCP-R, SCP-L, and ICP-R measurements did not show a statistically significant difference between the preoperative patient group values and the postoperative patient group values ( $p > 0.05$ ).

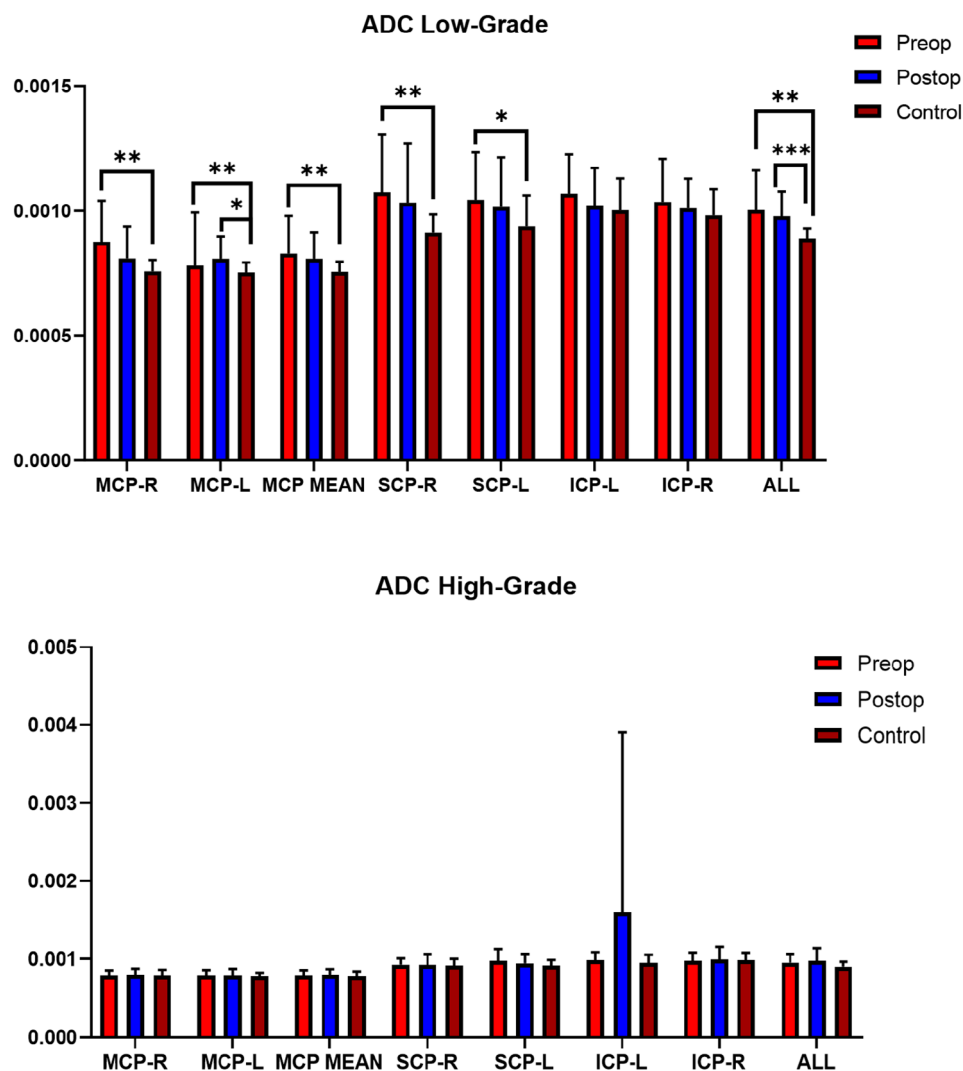


**FIGURE 7** The bar graph showing mean ADC values of the three groups in all regions. Statistical significances are indicated by asterisks. \* $p < 0.05$ ; \*\* $p < 0.01$ ; \*\*\* $p < 0.001$ .

The MCP-R, MCP-L, MCP mean, ICP-L, and ICP-R values measured in the preoperative patient group were significantly higher than control group values ( $p < 0.05$ ). SCP-R and SCP-L measurements did not show a statistically significant difference between the preoperative patient group values and the control group values ( $p > 0.05$ ).

SCP-R values measured in the control group were significantly higher than the postoperative patient group values ( $p < 0.05$ ), while SCP-L measurements did not show a statistically significant difference between the postoperative patient group values and the control group values ( $p > 0.05$ ). The MCP-R, MCP-L, MCP mean, ICP-L, and ICP-R measurements did not show a statistically significant difference between the postoperative patient group values and the control group values ( $p > 0.05$ ).

## 4 | DISCUSSION

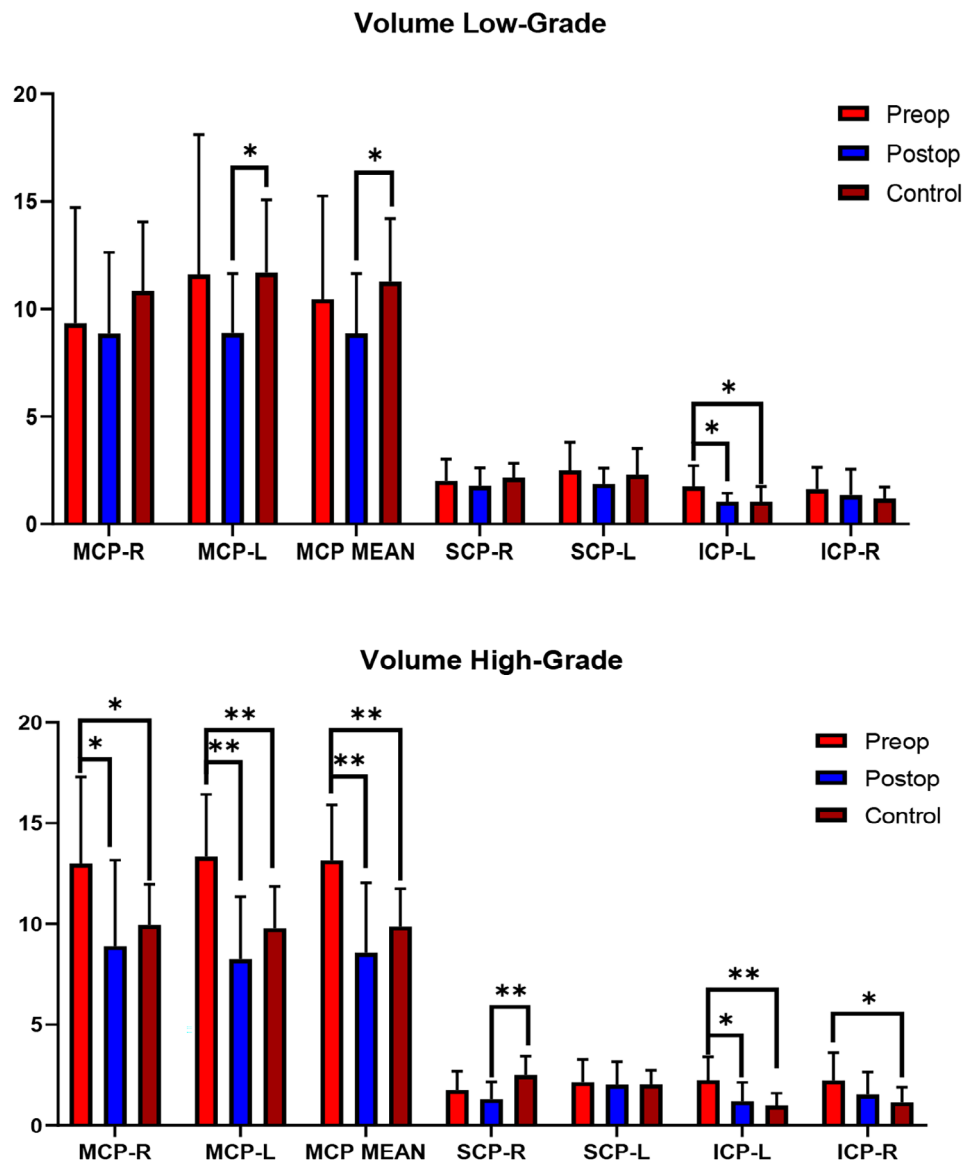
In this study, cerebellar pathways were studied with HARDI tractography in a group including toddlers to adolescents (1.5–16 y) with posterior fossa tumor and compared with age-sex matched

controls. In all tumor types and age groups, the superior cerebellar peduncle, which connects the cerebellar hemispheres and the mid-brain, was successfully identified. The MCP was identified as a single pathway group with two separate ROIs on the right and left. The inferior cerebellar peduncle, which carries fibers related to proprioception and balance, did not give very consistent results with the current technique in younger age groups. Fiber volume, FA, and ADC values were investigated for all three pathways.

### 4.1 | Diffusion imaging in neurosurgery

In its approach to brain tumors, neurosurgery aims both to provide maximum surgical resection and establish a balance regarding the preservation of functions (Dubey et al., 2018). Total resection of a tumor reduces the risk of recurrence and allows radiotherapy or chemotherapy to be more effective in the treatment process (Dubey et al., 2018). It also functionally preserves relevant regions of motor, visual or language functions, significantly improving the quality of life of these patients (Mandonnet et al., 2007). To achieve these goals,

**FIGURE 8** The bar graph showing mean fiber volume values of the three groups in all regions. Statistical significances are indicated by asterisks. \* $p < 0.05$ ; \*\* $p < 0.01$ .



many imaging modalities are used to evaluate brain tumors, such as conventional MRI, positron emission tomography, and functional MRI (fMRI) (Romano et al., 2007). In intracranial lesions, information about the structural integrity of some white matter tracts and tumor location is crucial for neurosurgery planning to identify the surgical access point and determine the affected areas of the brain and extent of tumor resection (Dubey et al., 2018). Diffusion tensor imaging is an important development in the field of diagnostic imaging. In fact, it is the only method that can demonstrate white matter tracts in vivo. It has previously been shown that this information can assist neurosurgeons in preoperative planning and postoperative evaluation (Yu et al., 2005).

Laundre et al. (Laundre et al., 2005) showed that the presence of motor deficits and the development of postoperative clinical normalization can be interpreted by identifying the corticospinal tract with the DTI method before operation. DTI may also contribute to clinical outcomes by preserving non-infiltrated white matter tracts. In their prospective study, Yu et al. (Yu et al., 2005) defined the relationship

of the tumor with the white matter pathways as simple displacement, displacement by infiltration, and simple deterioration. While performing maximum tumor resection in simple displacement, extensive resection preserved the residual part of the tract in those with simple disruption and displacement by infiltration (Yu et al., 2005). We have identified the tumor effects of edema, infiltration, displacement, and disruption in all subjects.

#### 4.2 | Evaluation of FA and ADC

When examining white matter changes, FA and ADC values are usually evaluated together (Won et al., 2016). ADC and FA provide information regarding the microstructure of the tissue (Assis et al., 2015; Gauvain et al., 2001).

It is known that the change of FA value is correlated with tumor cell density (Beppu et al., 2005; Goebell et al., 2006; Price et al., 2003; Won et al., 2016). Neoplastic cells and peritumoral edema cause

changes in brain structure. Typically, measurement of diffusion anisotropy from the normal brain parenchyma near the tumor indicates a decrease in FA values (Cruz Jr. & Sorensen, 2006). Studies have reported that FA values of Glioma III/IV decreased compared to control groups and this can be considered as tumor infiltration, while FA values were not changed in low grade tumors (Price et al., 2006). However, our results did not show a statistically significant change in FA values when all nerve pathways were compared between preoperatively, postoperatively, and between patients and control groups, neither in low-grade nor the high-grade tumor group.

Previous studies indicate an increase in ADC in the early stage without FA change (Morita et al., 2005; Price et al., 2003; Won et al., 2016), although another study reported no change in both parameters for low grade (Nilsson et al., 2007). Although many studies associate FA change with infiltration of tumor cells as a result of histological confirmation, there is limited information about ADC change only (Lee et al., 2008; Price et al., 2003).

Studies revealed a low ADC value with high tumor cellularity, which suggests a way of identification of low-grade tumors from high-grade (Pierce et al., 2014). As it is corresponding to the volume of the extracellular water compartment, ADC is sensitive over the changes of the cell density, edema, and necrosis (Wang et al., 2018). However, unfortunately, due to highly variable tissue and cell type of the type of the primary neoplasm, there is no consistent explanation of these parameters' changes. Our study revealed significantly higher ADC in some of the tracts as well as ALL tracts preoperatively, compared to postoperative ADC or to ADC in control groups in low-grade tumors but on the contrary not in high-grade tumors. Studies aiming to use these parameters as a potential clinical diagnostic tool, compared the preoperative ADC value over tumor grades and types. Recently, Darbar et al. showed that the mean lowest ADC value of the low-grade tumors were significantly higher than high-grade gliomas (Darbar et al., 2018).

Although a negative correlation has been established between glioma grade and ADC values in studies, it has been seen that the widespread application of ADC values to distinguish brain tumor types and grades results in inappropriate tumor classification (Rumboldt et al., 2006). ADC also fails to distinguish tumor tissue from peritumoral edema (Pauleit et al., 2004). On the other hand, ADC has been reported to be reliable for distinguishing specific tumor types such as dysembryoplastic neuroepithelial tumors and has also been reported to help characterize some pediatric brain tumors (Gauvain et al., 2001; Tzika et al., 2002). Additionally, preoperative diffusion values can predict tumor response to radiation therapy and are important in distinguishing radiation-induced brain injury from tumor recurrence (Asao et al., 2005; Mardor et al., 2004).

Many studies focused on the various components of the peritumoral regions, and a variety of decreased, increased, constant FA and ADC values combinations were reported. The variative results may result from the heterogeneous biology of the neoplasms and the subjective locations of the placed ROIs (Field et al., 2004). It is also suggested that, different tracts may be responding differently (Field et al., 2004). Another aspect is that, in general, studies focusing on

cerebral neoplasm use the contralateral unaffected region as a control. However, this was not possible in this study because of the heterogeneous locations of the tumors around the cerebellum, so we used age- and sex-matched another subject for comparison.

### 4.3 | Effects of the tumor in white matter tracts

Low-grade gliomas are characterized by displacement rather than destruction of surrounding white matter fibers. Low-grade neoplasms are well-circumscribed lesions that do not cause invasion or disruption of nerve pathways. These lesions tend to deviate to the surrounding white matter fibers (Cruz Jr. & Sorensen, 2006). Metastasis and meningiomas have also been reported to cause displacement rather than infiltration in adjacent white matter pathways (Cruz Jr. & Sorensen, 2006).

When our samples were examined morphologically, it was observed that the 'displacement' in the tracts which Yu et al. (Yu et al., 2005) defined as type 1 was greatly reduced after the operation. However, cases with a decrease in fiber volume due to tumor resection after the operation were thought to be associated with tumor infiltration. Our study revealed significantly decreased volume of fibers in some of the regions preoperatively and postoperatively and controls both in low- and high-grade tumors. In these regions, loss of fibers can be considered a result of tumor resection.

### 4.4 | Evaluation of the postoperative results

The posterior fossa tumors are considered very critical because of the limited space of the posterior cranial fossa and possible effects on vital nuclei in the brainstem (Prasad et al., 2017). The presence of a tumor in this area will reveal functional symptoms related to the brain stem, cerebellum, and hydrocephalus (Sönmez et al., 2012). It is stated that neurological findings vary according to the location of the tumor and the age of the patient (Sönmez et al., 2012). However, the symptoms and signs are primarily due to increased intracranial pressure, followed by compression of the cerebellum nuclei and brainstem structures. In tumors affecting the pontocerebellar angle, clinical findings for cranial nerves (CN V, CN VII, and CN VIII) might be observed because of their dysfunction (Sönmez et al., 2012). It has been reported that trunk and gait ataxia is observed in cerebellum tumors located in the midline, while findings such as dysmetria, extremity ataxia, nystagmus, hypotonia, and hyporeflexia are observed in those located in the cerebellar hemispheres (Gilman, 1981; Sönmez et al., 2012). The most important indicators of pediatric infratentorial localized tumors are severe headache, vomiting, and blurred vision because of increased intracranial pressure and associated hydrocephalus (Grondin et al., 2009). Our preoperative diagnostic reports revealed a variety of symptoms in accordance with the site of the tumor from mild to severe conditions (Table 2).

Posterior fossa syndrome (PFS) is a collection of neurological symptoms seen in 8%–32% cases after the tumor resection of the



posterior fossa (Wahab et al., 2016; Yecies et al., 2019). PFS is also called cerebellar mutism, cerebellar speech syndrome, cerebellar mutism and subsequent dysarthria, and cerebellar cognitive affective syndrome (Yecies et al., 2019). The symptoms of PFS generally recover in time but speech impairment and ataxia may reside as residual symptoms after the surgery (Yecies et al., 2019). According to our patient reports, only one of the 30 patients (s14) experienced PFS for one day and could not remember anyone, but the patient later showed improvement.

Postoperative notes belonging to our patient group stated that most of them improved in terms of headache and ataxia after the operation. However, two patients had diplopia (s6 and s17), one had mild incoordination (s8), one had delayed gross and fine motor and language responses (s39), three had mild balance problems (s9, s12, and s21), and one patient had a right-sided motor weakness (s6). It was reported that one of the children (s40) had low-to-moderate cognitive abilities after the operation, and another had concentration problems (s28). Only one case with pilocytic astrocytoma at the cervicomedullary junction (s37) was included in the study and this patient experienced vocal cord weakness after the operation.

## 5 | LIMITATIONS

There are some limitations due to the retrospective nature of the study. The most important is that patients cannot be separated according to the type of pathology, and site of the lesion due to the limited number of subjects in each group. An additional limitation of this study is that the age distributions of available participants for the groups in this experiment vary considerably, because of the availability of appropriate participants that met our inclusion criteria from a large clinical population. This inevitably resulted in imbalanced pools of participants for further analysis. Thus, we were not also able to compare among sexes and age groups. In our future study, we are planning to address these limitations.

We were also able to use the scan 3 months after the surgery as the postoperative scanning. Even though there were patients followed up on annually in the current hospital, some of them were not. Further analysis of follow up scanning is warranted as future work.

## 6 | CONCLUSIONS

Conventional MR techniques (T2-weighted, T1-weighted, and FLAIR) are widely used for radiological evaluation and localization of brain tumors. However, these MRI methods cannot provide precise information about the integrity and location of the white matter tracts in the immediate region surrounding the tumors. Diffusion imaging and tractography are important in determining tumor spread, in terms of qualitative and quantitative demonstration of nerve pathways. This study showed that the effects of tumors on cerebellar peduncles and the nerve fibers passing through it can be successfully evaluated with HARDI tractography. The technique has been shown to be useful not only in neurosurgery planning but also in postoperative evaluation.

## ACKNOWLEDGMENTS

This study was presented as an oral presentation at 37th Annual Meeting of the American Association of Clinical Anatomists, June 15–19, 2020, and the abstract was published with DOI: 10.1002/ca.23694. Authors would like to thank Dr Jose Luis Alatorre Warren for his help in manuscript preparation.

## FUNDING INFORMATION

This work was sponsored by Grant No. 2018/14 from the Research Fund of Istanbul Medipol University to AO and NY (Thesis Supervisor) as a part of PhD Dissertation Project. This work was also supported by the National Institutes of Health (grant numbers R01HD078561, R01NS109475) to ET.

## CONFLICT OF INTEREST

The authors declare that they have no conflict of interest.

## ORCID

Alpen Ortug  <https://orcid.org/0000-0002-6813-8351>

## REFERENCES

- Akhlaghi, H., Yu, J., Corben, L., Georgiou-Karistianis, N., Bradshaw, J. L., Storey, E., Delatycki, M. B., & Egan, G. F. (2014). Cognitive deficits in Friedreich ataxia correlate with micro-structural changes in dentatoruber tract. *The Cerebellum*, 13(2), 187–198.
- Albright, L. (1992). Posterior fossa tumors. *Neurosurgery Clinics*, 3(4), 881–891.
- Asao, C., Korogi, Y., Kitajima, M., Hirai, T., Baba, Y., Makino, K., Kochi, M., Morishita, S., & Yamashita, Y. (2005). Diffusion-weighted imaging of radiation-induced brain injury for differentiation from tumor recurrence. *AJNR. American Journal of Neuroradiology*, 26(6), 1455–1460.
- Assis, Z. A., Saini, J., Ranjan, M., Gupta, A. K., Sabharwal, P., & Naidu, P. R. (2015). Diffusion tensor imaging in evaluation of posterior fossa tumors in children on a 3T MRI scanner. *The Indian Journal of Radiology & Imaging*, 25(4), 445–452. <https://doi.org/10.4103/0971-3026.169444>
- Beppu, T., Inoue, T., Shibata, Y., Yamada, N., Kurose, A., Ogasawara, K., Ogawa, A., & Kabasawa, H. (2005). Fractional anisotropy value by diffusion tensor magnetic resonance imaging as a predictor of cell density and proliferation activity of glioblastomas. *Surgical Neurology*, 63(1), 56–61. <https://doi.org/10.1016/j.surneu.2004.02.034>
- Berman, J. I., Lanza, M. R., Blaskey, L., Edgar, J. C., & Roberts, T. P. L. (2013). High angular resolution diffusion imaging probabilistic tractography of the auditory radiation. *American Journal of Neuroradiology*, 34(8), 1573–1578. <https://doi.org/10.3174/ajnr.A3471>
- Black, P. M. (2000). The present and future of cerebral tumor surgery in children. *Child's Nervous System*, 16(10–11), 821–828.
- Bulakbasi, N. (2009). Diffusion-tensor imaging in brain tumors. *Imaging in Medicine*, 1(2), 155–171.
- Celtikci, P., Fernandes-Cabral, D. T., Yeh, F. C., Panesar, S. S., & Fernandez-Miranda, J. C. (2018). Generalized q-sampling imaging fiber tractography reveals displacement and infiltration of fiber tracts in low-grade gliomas. *Neuroradiology*, 60(3), 267–280. <https://doi.org/10.1007/s00234-018-1985-5>
- Cruz, L. C., Jr., & Sorensen, A. G. (2006). Diffusion tensor magnetic resonance imaging of brain tumors. *Magnetic Resonance Imaging Clinics of North America*, 14(2), 183–202. <https://doi.org/10.1016/j.mric.2006.06.003>
- Darbar, A., Waqas, M., Enam, S. F., & Mahmood, S. D. (2018). Use of pre-operative apparent diffusion coefficients to predict brain tumor grade. *Cureus*, 10(3), e2284. <https://doi.org/10.7759/cureus.2284>

- Dubey, A., Kataria, R., & Sinha, V. D. (2018). Role of diffusion tensor imaging in brain tumor surgery. *Asian Journal of Neurosurgery*, 13(2), 302–306.
- Essayed, W. I., Zhang, F., Unadkat, P., Cosgrove, G. R., Golby, A. J., & O'Donnell, L. J. (2017). White matter tractography for neurosurgical planning: A topography-based review of the current state of the art. *NeuroImage*, 15, 659–672. <https://doi.org/10.1016/j.neuroimage.2017.06.011>
- Farquharson, S., Tournier, J. D., Calamante, F., Fabin, G., Schneider-Kolsky, M., Jackson, G. D., & Connelly, A. (2013). White matter fiber tractography: Why we need to move beyond DTI. *Journal of Neurosurgery*, 118(6), 1367–1377. <https://doi.org/10.3171/2013.2.jns121294>
- Field, A. S., Alexander, A. L., Wu, Y.-C., Hasan, K. M., Witwer, B., & Badie, B. (2004). Diffusion tensor eigenvector directional color imaging patterns in the evaluation of cerebral white matter tracts altered by tumor. *Journal of Magnetic Resonance Imaging*, 20(4), 555–562. <https://doi.org/10.1002/jmri.20169>
- Gauvain, K. M., McKinstry, R. C., Mukherjee, P., Perry, A., Neil, J. J., Kaufman, B. A., & Hayashi, R. J. (2001). Evaluating pediatric brain tumor cellularity with diffusion-tensor imaging. *AJR. American Journal of Roentgenology*, 177(2), 449–454. <https://doi.org/10.2214/ajr.177.2.1770449>
- Gilman, S. (1981). *Disorders of the cerebellum*. F.A. Davis Co.
- Goebell, E., Fiehler, J., Ding, X. Q., Paustenbach, S., Nietz, S., Heese, O., ... Zeumer, H. (2006). Disarrangement of fiber tracts and decline of neuronal density correlate in glioma patients—A combined diffusion tensor imaging and 1H-MR spectroscopy study. *American Journal of Neuroradiology: AJNR*, 27(7), 1426–1431.
- Grondin, R. T., Scott, R. M., & Smith, E. R. (2009). Pediatric brain tumors. *Advances in Pediatrics*, 56(1), 249–269. <https://doi.org/10.1016/j.yapd.2009.08.006>
- Huisman, T. A. G. M. (2010). Diffusion-weighted and diffusion tensor imaging of the brain, made easy. *Cancer Imaging*, 10, S163–S171. <https://doi.org/10.1102/1470-7330.2010.9023>
- Ibrahim, A. S., Gomaa, M., Sakr, H., & Elzaher, Y. A. (2013). Role of diffusion tensor imaging in characterization and preoperative planning of brain neoplasms. *The Egyptian Journal of Radiology and Nuclear Medicine*, 44(2), 297–307.
- Jin, Z., Bao, Y., Wang, Y., Li, Z., Zheng, X., Long, S., & Wang, Y. (2019). Differences between generalized Q-sampling imaging and diffusion tensor imaging in visualization of crossing neural fibers in the brain. *Surgical and Radiologic Anatomy*, 41(9), 1019–1028. <https://doi.org/10.1007/s00276-019-02264-1>
- Kamali, A., Kramer, L. A., Frye, R. E., Butler, I. J., & Hasan, K. M. (2010). Diffusion tensor tractography of the human brain cortico-ponto-cerebellar pathways: A quantitative preliminary study. *Journal of Magnetic Resonance Imaging*, 32(4), 809–817.
- Karimi, S., Petrovich, N. M., Peck, K. K., Hou, B. L., & Holodny, A. I. (2006). Advanced MR techniques in brain tumor imaging. *Applied Radiology*, 35(5), 9–18.
- Keser, Z., Hasan, K. M., Mwangi, B. I., Kamali, A., Ucisik-Keser, F. E., Riascos, R. F., ... Narayana, P. A. (2015). Diffusion tensor imaging of the human cerebellar pathways and their interplay with cerebral macrostructure. *Frontiers in Neuroanatomy*, 9, 41. <https://doi.org/10.3389/fnana.2015.00041>
- Laundre, B. J., Jellison, B. J., Badie, B., Alexander, A. L., & Field, A. S. (2005). Diffusion tensor imaging of the corticospinal tract before and after mass resection as correlated with clinical motor findings: Preliminary data. *AJNR. American Journal of Neuroradiology*, 26(4), 791–796.
- Lee, H. Y., Na, D. G., Song, I. C., Lee, D. H., Seo, H. S., Kim, J. H., & Chang, K. H. (2008). Diffusion-tensor imaging for glioma grading at 3-T magnetic resonance imaging: Analysis of fractional anisotropy and mean diffusivity. *Journal of Computer Assisted Tomography*, 32(2), 298–303. <https://doi.org/10.1097/RCT.0b013e318076b44d>
- Leitner, Y., Travis, K. E., Ben-Shachar, M., Yeom, K. W., & Feldman, H. M. (2015). Tract profiles of the cerebellar white matter pathways in children and adolescents. *Cerebellum*, 14(6), 613–623. <https://doi.org/10.1007/s12311-015-0652-1>
- Lope-Piedrafita, S. (2018). Diffusion tensor imaging (DTI). In *preclinical MRI* (pp. 103–116). Springer.
- Ma, J., Su, S., Yue, S., Zhao, Y., Li, Y., Chen, X., & Ma, H. (2016). Preoperative visualization of cranial nerves in skull base tumor surgery using diffusion tensor imaging technology. *Turkish Neurosurgery*, 26(6), 805–812.
- Mandonnet, E., Jabbi, S., Taillandier, L., Galanaud, D., Benali, H., Capelle, L., & Duffau, H. (2007). Preoperative estimation of residual volume for WHO grade II glioma resected with intraoperative functional mapping. *Neuro-Oncology*, 9(1), 63–69. <https://doi.org/10.1215/15228517-2006-015>
- Mardor, Y., Roth, Y., Ochershvilli, A., Spiegelmann, R., Tichler, T., Daniels, D., Maier, S. E., Nissim, O., Ram, Z., Baram, J., Orenstein, A., & Pfeffer, R. (2004). Pretreatment prediction of brain tumors' response to radiation therapy using high b-value diffusion-weighted MRI. *Neoplasia*, 6(2), 136–142. <https://doi.org/10.1593/neo.03349>
- McEvoy, S. D., Lee, A., Poliakov, A., Friedman, S., Shaw, D., Browd, S. R., Ellenbogen, R. G., Ojemann, J. G., & Mac Donald, C. L. (2016). Longitudinal cerebellar diffusion tensor imaging changes in posterior fossa syndrome. *NeuroImage: Clinical*, 12, 582–590. <https://doi.org/10.1016/j.neuroimage.2016.09.007>
- Meola, A., Comert, A., Yeh, F. C., Sivakanthan, S., & Fernandez-Miranda, J. C. (2016). The nondecussating pathway of the dentatorubrothalamic tract in humans: Human connectome-based tractographic study and microdissection validation. *Journal of Neurosurgery*, 124(5), 1406–1412. <https://doi.org/10.3171/2015.4.Jns142741>
- Mori, S., Wakana, S., Nagae-Poetscher, L., & van Zijl, P. (2005). *MRI atlas of human white matter*. Elsevier.
- Morita, K., Matsuzawa, H., Fujii, Y., Tanaka, R., Kwee, I. L., & Nakada, T. (2005). Diffusion tensor analysis of peritumoral edema using lambda chart analysis indicative of the heterogeneity of the microstructure within edema. *Journal of Neurosurgery*, 102(2), 336–341. <https://doi.org/10.3171/jns.2005.102.2.0336>
- Nilsson, D., Rutka, J. T., Snead, O. C., Raybaud, C. R., & Widjaja, E. (2007). Preserved structural integrity of white matter adjacent to low-grade tumors. *Child's Nervous System*, 24(3), 313–320. <https://doi.org/10.1007/s00381-007-0466-7>
- Oh, M. E., Driever, P. H., Khajuria, R. K., Rueckriegel, S. M., Koustenis, E., Bruhn, H., & Thomale, U.-W. (2017). DTI fiber tractography of cerebro-cerebellar pathways and clinical evaluation of ataxia in childhood posterior fossa tumor survivors. *Evaluation of Neuro-Oncology*, 13(2), 267–276. <https://doi.org/10.1007/s11060-016-2290-y>
- Packer, R. J., Friedman, H. S., Kun, L. E., & Fuller, G. N. (2002). Tumors of the brain stem, cerebellum, and fourth ventricle. In V. A. Levin (Ed.), *Cancer in the nervous system* (2nd Ed., 171–192). New York: Oxford University Press.
- Pauleit, D., Langen, K. J., Floeth, F., Hautzel, H., Riemenschneider, M. J., Reifenberger, G., ... Muller, H. W. (2004). Can the apparent diffusion coefficient be used as a noninvasive parameter to distinguish tumor tissue from peritumoral tissue in cerebral gliomas? *Journal of Magnetic Resonance Imaging*, 20(5), 758–764. <https://doi.org/10.1002/jmri.20177>
- Pierce, T., Kranz, P. G., Roth, C., Leong, D., Wei, P., & Provenzale, J. M. (2014). Use of apparent diffusion coefficient values for diagnosis of pediatric posterior fossa tumors. *The Neuroradiology Journal*, 27(2), 233–244. <https://doi.org/10.15274/NRJ-2014-10027>
- Potgieser, A. R., Wagemakers, M., van Hulzen, A. L., de Jong, B. M., Hoving, E. W., & Groen, R. J. (2014). The role of diffusion tensor imaging in brain tumor surgery: A review of the literature. *Clinical Neurology and Neurosurgery*, 124, 51–58. <https://doi.org/10.1016/j.clineuro.2014.06.009>

- Prasad, K. S. V., Ravi, D., Pallikonda, V., & Raman, B. V. S. (2017). Clinico-pathological study of pediatric posterior fossa tumors. *Journal of Pediatric Neurosciences*, 12(3), 245–250. [https://doi.org/10.4103/jpn.JPN\\_113\\_16](https://doi.org/10.4103/jpn.JPN_113_16)
- Price, S. J., Burnet, N. G., Donovan, T., Green, H. A., Pena, A., Antoun, N. M., Pickard, J. D., Carpenter, T. A., & Gillard, J. H. (2003). Diffusion tensor imaging of brain tumours at 3T: A potential tool for assessing white matter tract invasion? *Clinical Radiology*, 58(6), 455–462. [https://doi.org/10.1016/s0009-9260\(03\)00115-6](https://doi.org/10.1016/s0009-9260(03)00115-6)
- Price, S. J., Jena, R., Burnet, N. G., Hutchinson, P. J., Dean, A. F., Pena, A., Pickard, J. D., Carpenter, T. A., & Gillard, J. H. (2006). Improved delineation of glioma margins and regions of infiltration with the use of diffusion tensor imaging: An image-guided biopsy study. *AJNR. American Journal of Neuroradiology*, 27(9), 1969–1974.
- Re, T. J., Levman, J., Lim, A. R., Righini, A., Grant, P. E., & Takahashi, E. (2017). High-angular resolution diffusion imaging tractography of cerebellar pathways from newborns to young adults. *Brain and Behavior: A Cognitive Neuroscience Perspective*, 7(1), e00589. <https://doi.org/10.1002/brb3.589>
- Romano, A., Ferrante, M., Cipriani, V., Fasoli, F., Ferrante, L., D'Andrea, G., Fantozzi, L. M., & Bozzao, A. (2007). Role of magnetic resonance tractography in the preoperative planning and intraoperative assessment of patients with intra-axial brain tumours. *La Radiologia Medica*, 112(6), 906–920. <https://doi.org/10.1007/s11547-007-0181-1>
- Rumboldt, Z., Camacho, D. L., Lake, D., Welsh, C. T., & Castillo, M. (2006). Apparent diffusion coefficients for differentiation of cerebellar tumors in children. *AJNR. American Journal of Neuroradiology*, 27(6), 1362–1369.
- Salama, G. R., Heier, L. A., Patel, P., Ramakrishna, R., Magge, R., & Tsiouris, A. J. (2017). Diffusion weighted/tensor imaging, functional MRI and perfusion weighted imaging in glioblastoma-foundations and future. *Frontiers in Neurology*, 8, 660. <https://doi.org/10.3389/fneur.2017.00660>
- Sönmez, M. A., Tekiner, A., Bayar, M. A., & Yilmaz, A. (2012). Posterior Fossa İntraaksiyel Tümörlerinin Retrospektif İncelenmesi. *Kocatepe Tıp Dergisi*, 13(3), 133–137.
- Tae, W.-S., Ham, B.-J., Pyun, S.-B., Kang, S.-H., & Kim, B.-J. (2018). Current clinical applications of diffusion-tensor imaging in neurological disorders. *Journal of Clinical Neurology*, 14(2), 129–140.
- Tuch, D. S. (2004). Q-ball imaging. *Magnetic Resonance in Medicine*, 52(6), 1358–1372. <https://doi.org/10.1002/mrm.20279>
- Tzika, A. A., Zarifi, M. K., Goumnerova, L., Astrakas, L. G., Zurakowski, D., Young-Poussaint, T., Anthony, D. C., Scott, R. M., & Black, P. M. (2002). Neuroimaging in pediatric brain tumors: Gd-DTPA-enhanced, hemodynamic, and diffusion MR imaging compared with MR spectroscopic imaging. *AJNR. American Journal of Neuroradiology*, 23(2), 322–333.
- Vedantam, A., Stormes, K. M., Gadgil, N., Kralik, S. F., Aldave, G., & Lam, S. K. (2019). Association between postoperative DTI metrics and neurological deficits after posterior fossa tumor resection in children. *Journal of Neurosurgery Pediatrics*, 1-7, 364–370. <https://doi.org/10.3171/2019.5.Peds1912>
- Wahab, S. S., Hettige, S., Mankad, K., & Aquilina, K. (2016). Posterior fossa syndrome-a narrative review. *Quantitative Imaging in Medicine and Surgery*, 6(5), 582–590. <https://doi.org/10.21037/qims.2016.10.12>
- Wang, S., Meng, M., Zhang, X., Wu, C., Wang, R., Wu, J., ... Xu, K. (2018). Texture analysis of diffusion weighted imaging for the evaluation of glioma heterogeneity based on different regions of interest. *Oncology Letters*, 15(5), 7297–7304. <https://doi.org/10.3892/ol.2018.8232>
- Witwer, B. P., Moftakhar, R., Hasan, K. M., Deshmukh, P., Haughton, V., Field, A., Chen, L., & Badie, B. (2002). Diffusion-tensor imaging of white matter tracts in patients with cerebral neoplasm. *Journal of Neurosurgery*, 97(3), 568–575. <https://doi.org/10.3171/jns.2002.97.3.0568>
- Won, Y. I., Chung, C. K., Kim, C. H., Park, C.-K., Koo, B.-B., Lee, J.-M., & Jung, H.-W. (2016). White matter change revealed by diffusion tensor imaging in gliomas. *Brain Tumor Research and Treatment*, 4(2), 100–106. <https://doi.org/10.14791/btrt.2016.4.2.100>
- Yecies, D., Jabarkheel, R., Han, M., Kim, Y.-H., Bruckert, L., Shpanskaya, K., Perez, A., Edwards, M. S. B., Grant, G. A., & Yeom, K. W. (2019). Posterior fossa syndrome and increased mean diffusivity in the olivary bodies. *Journal of Neurosurgery. Pediatrics*, 24(4), 376–381. <https://doi.org/10.3171/2019.5.PEDS1964>
- Yen, P. S., Teo, B. T., Chiu, C. H., Chen, S. C., Chiu, T. L., & Su, C. F. (2009). White matter tract involvement in brain tumors: A diffusion tensor imaging analysis. *Surgical Neurology*, 72(5), 464–469. <https://doi.org/10.1016/j.surneu.2009.05.008>
- Yu, C. S., Li, K. C., Xuan, Y., Ji, X. M., & Qin, W. (2005). Diffusion tensor tractography in patients with cerebral tumors: A helpful technique for neurosurgical planning and postoperative assessment. *European Journal of Radiology*, 56(2), 197–204. <https://doi.org/10.1016/j.ejrad.2005.04.010>

## SUPPORTING INFORMATION

Additional supporting information may be found in the online version of the article at the publisher's website.

**How to cite this article:** Ortug, A., Yuzbasioglu, N., Akalan, N., Levman, J., & Takahashi, E. (2022). Preoperative and postoperative high angular resolution diffusion imaging tractography of cerebellar pathways in posterior fossa tumors. *Clinical Anatomy*, 35(8), 1085–1099. <https://doi.org/10.1002/ca.23914>